Available online at www.sciencedirect.com
SCIENCE DIRECT®
PERGAMON
International Journal of Heat and Mass Transfer 46 (2003) 3683–3695
International Journal of HEAT and MASS TRANSFER
www.elsevier.com/locate/ijhmt

Validation of the use of heat transfer models in liquid/solid fluidized beds for ice slurry generation

J.W. Meewisse *, C.A. Infante Ferreira [1]

Refrigeration Engineering and Indoor Climate Technology, Delft University of Technology, Mekelweg 2, 2628 CD Delft, The Netherlands

Received 20 September 2002; received in revised form 6 March 2003

Abstract

Heat transfer coefficients in a liquid/solid fluidized bed heat exchanger are investigated for application in ice slurry generators. A range of temperature driving forces is determined in which ice slurry generation is stable. In this range ice crystal formation or growth does not affect heat transfer coefficients. A model is proposed that accurately predicts heat transfer coefficients in the fluidized bed ice slurry generator. Due to lower temperatures and higher viscosity in ice slurry generation, heat transfer coefficients measured are lower than predicted with heat transfer correlations specific for liquid/solid fluidized bed heat exchangers. Heat transfer coefficients measured are however significantly higher than for single phase fluid flow.

Keywords: Fluidized beds; Heat transfer; Phase change

1. Introduction

Application of ice slurries as secondary cooling fluids in food industry and in air-conditioning has gained increasing attention in recent years [1–4]. These are used as cold carrier fluids to reduce both primary refrigerant load and also safety and environmental hazards involved with primary refrigerants such as ammonia, hydrocarbons or HFCs. Furthermore, storage of ice slurries produced during the night for the use in cooling applications during the day allows for leveling and shifting of electrical power loads.

Ice slurries consist of mixtures of water with a freezing point depressing additive in which small ice crystals with mean diameter of 0.1–3 mm are present. The diameters of ice crystals depend on the type of ice slurry generation and storage method. Freezing point depressants are either inorganic substances, like sodium chloride, or organic substances, such as ethanol or ethylene glycol.

Ice slurries are advantageous because of the latent heat effect involved with ice formation. The apparent heat capacity is much higher than if only the sensible heat effect of fluids without phase change is used. Major drawback of the ice slurry systems has been the high cost associated with the ice slurry generator. An alternative ice slurry generator that reduces initial investment cost and may improve heat transfer coefficients and lower maintenance cost is sought in a fluidized bed heat exchanger.

Fluidized bed heat exchangers are used to prevent fouling in various process applications [5,6]. These heat exchangers consist of one or several parallel tubes with heated or cooled walls. Inert solid particles are fluidized inside the tubes. In an ice slurry generator the walls are cooled by evaporation of a primary refrigerant such as a HFC, ammonia or a hydrocarbon. The solid particles are fluidized by the ice slurry feed flow. After the feed flow is supercooled below its freezing point in the fluidized bed, initial nucleation takes place and ice crystal growth starts. Solid particles prevent build-up of a solid

* Corresponding author. Tel.: +31-15-278-6669; fax: +31-15-278-7204.

E-mail addresses: j.w.meewisse@wbmt.tudelft.nl (J.W. Meewisse), c.a.infanteferreira@wbmt.tudelft.nl (C.A. Infante Ferreira).

[1] Tel.: +31-15-278-4894; fax: +31-15-278-2460.

0017-9310/03/$ - see front matter © 2003 Elsevier Ltd. All rights reserved.
doi:10.1016/S0017-9310(03)00171-6

Nomenclature

A	heat transfer surface area (m^2)
Ar	Archimedes number ($g \cdot d_p^3 \rho_l \cdot (\rho_s - \rho_l)/\mu^2$) (–)
$c_{1,\ldots,7}$	constant coefficients (–)
c_p	heat capacity (J/kg K)
c_{p_app}	apparent heat capacity (incl. latent heat effect) (J/kg K)
d	tube diameter (m)
d_p	equivalent particle diameter (diameter of a sphere of equal volume) (m)
D	bed diameter (m)
g	gravitational acceleration (m/s^2)
h	enthalpy (J/kg)
ΔH_f	enthalpy of fusion (J/kg)
m	concentration in liquid phase (kg/kg solution)
Nu_p	Nusselt number ($= \alpha \cdot d_p/\lambda$) (–)
Nu_h	hydraulic Nusselt number ($= Nu_p \cdot \varepsilon/(1-\varepsilon)$) (–)
Pr	Prandtl number ($\mu \cdot c_p/\lambda$) (–)
Q	Heat transfer rate (W)
Re_p	Reynolds number ($= \rho \cdot u_s \cdot d_p/\mu$) (–)
Re_h	hydraulic Reynolds number ($= Re_p/(1-\varepsilon)$) (–)
T	temperature (°C)
T_f	freezing temperature (°C)
ΔT	(maximum) temperature difference (K)
ΔT_{ln}	logarithmic mean temperature difference (K)
U	overall heat transfer coefficient (W/m^2 K)
u_s	superficial velocity (m/s)
w_i	weight fraction of ice (kg/kg)

Greek symbols

α	wall-to-bed heat transfer coefficient (W/m^2 K)
ε	bed voidage (–)
λ	thermal conductivity (W/m K)
μ	dynamic viscosity (Pa s)
ρ	density (kg/m^3)
ϕ_i	volumetric ice fraction (m^3/m^3)

Subscripts

i	ice
in	inside
is	ice slurry
fpd	freezing point depressant
l	liquid
out	outside
p	particle
s	solid
w	wall

ice layer on the heat transfer surfaces and also enhance heat transfer coefficients [7]. Maximum size of ice crystals produced is limited by the continuous interactions with solid particles of the fluidized bed [8]. A section is installed on top of the fluidized bed heat exchanger to separate the solid particles from the ice slurry. The fluidized beds can either operate stationary or with recirculation of the solid particles through a downcomer pipe. A schematic layout of a fluidized bed system with an evaporating primary refrigerant is given in Fig. 1.

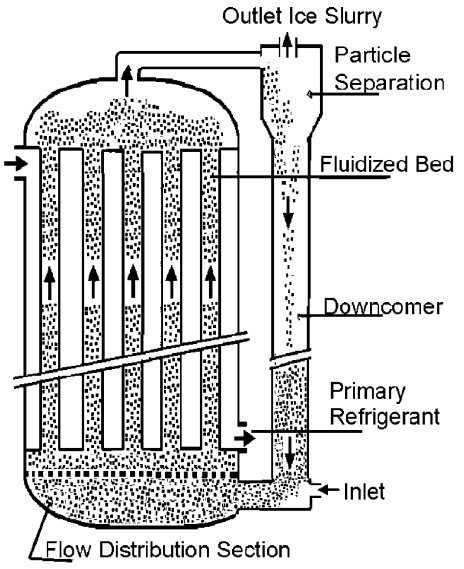

Fig. 1. Schematic layout of a fluidized bed ice slurry generator.

This research aims to determine heat transfer coefficients in stationary fluidized bed heat exchangers applied for ice slurry generation. Heat transfer coefficients would characterize the mechanism of ice slurry formation in the fluidized bed ice slurry generator.

Numerous correlations of wall to fluidized bed heat transfer have been reported [7,9,10]. The literature correlations will be examined experimentally for the specific case of ice slurry generation, after which a heat transfer model will be developed for ice slurry generation in fluidized beds.

2. Heat transfer in fluidized bed ice slurry generators

2.1. Heat transfer mechanisms

Wall-to-bed heat transfer coefficients are higher compared to those in pipes without particles [7]. This is caused by three enhancement mechanisms:

1. The solid particles break up the laminar boundary layer that has a large heat transfer resistance. This positive effect is expected to be dominant during ice crystallization.
2. The solid particles transfer heat by conduction during direct contact with the walls. This positive effect may be reduced by the presence of ice crystals, if the ice crystals prevent contact of particles with the walls. This effect is particularly important in gas/solid fluidized beds and in liquid/solid fluidized beds with dense and highly conductive solid particles as copper [25].
3. The heat exchanging walls are kept clear of fouling. This effect is the main reason to apply fluidized bed heat exchangers in various process applications with severely fouling process fluids [8]. The solid particle impacts prevent the build-up of a permanent ice layer at the heat exchanger walls.

The exact heat transfer mechanism is not known for wall-to-bed heat transfer in a fluidized bed ice slurry generator. The presence of ice crystals probably affects heat transfer. Several possibilities are distinguished:

1. There are no effects of the ice crystals. Heat transfer coefficients will be as in regular liquid/solid fluidized beds. Properties of the liquid phase of the ice slurry are required to predict heat transfer coefficients.
2. The ice crystals interfere with heat transfer coefficients, but do not stick to the heat transfer surfaces. The ice slurry can be regarded as a single fluid.
3. There is a semi-permanent layer of ice at the heat transfer surfaces. Ice crystals are removed continuously by the mechanical impact of solid particles of the fluidized bed.
4. A combination is also possible: Heat transfer coefficients may be affected by ice crystals, while there also is a semi-permanent ice layer stuck to walls.

Heat transfer coefficients may also be affected by varying local ice fractions. Ice crystals may be formed principally in the laminar boundary layer near walls. Slow mass transfer of ice crystals to the bulk of the fluidized bed might then result in an uneven distribution of ice crystals.

By measuring heat transfer coefficients from wall-to-bed, an attempt is made to determine the heat transfer mechanism. Heat transfer models for liquid/solid fluidized bed heat exchangers are used as starting point for this evaluation. Thermophysical properties of liquid phase and ice slurry as a whole are examined in the models, to determine which properties are significant and which heat transfer mechanism prevails.

Heat transfer measurements may result in a better understanding of the ice formation mechanism. If during ice formation there is a semi-permanent ice layer sticking to the walls, heat transfer coefficients are expected to be significantly lower compared to liquid/solid fluidized bed heat transfer under similar conditions where no ice crystals are formed. In experiments these conditions are obtained just before the start of ice crystallization, therefore comparison of heat transfer coefficients with and without crystallization follows from the experiments.

2.2. Ice slurry properties

Various property models have been used in calculations of ice slurry systems [2,11]. Models used by different researchers yield a wide range of errors, which are made when the ice slurry is seen as a single fluid. Influence of properties such as size and shape of individual ice crystals is then disregarded. The following set of thermophysical property models have been applied by various researchers.

Density of ice slurries is calculated by weighted addition of the density of pure ice and the density of the solution. At higher ice fractions the density of the ice slurry decreases.

$$\rho_{is} = \frac{1}{w_i/\rho_i + (1 - w_i)/\rho_l} \tag{1}$$

Several researchers have investigated the *thermal conductivity* of solid/liquid mixtures. Ben Lakhdar [12] has shown that the model proposed by Tareef [13] yields satisfactory results for ethanol ice slurries up to an ice volume fraction of 0.4:

$$\lambda_{is} = \lambda_l \cdot \left(\frac{2 \cdot \lambda_l + \lambda_i - 2 \cdot \phi_i \cdot (\lambda_l - \lambda_i)}{2 \cdot \lambda_l + \lambda_i + \phi_i \cdot (\lambda_l - \lambda_i)} \right) \tag{2}$$

The model has not been experimentally validated directly, due to the absence of a reliable thermal conductivity measurement method for ice slurries. At increasing ice fractions, the thermal conductivity of the ice slurry will increase according to Eq. (2).

Enthalpy of ice slurries is given by:

$$h_{is}(T) = w_i(T) \cdot [h_i(T) - \Delta H_f] + [1 - w_i(T)] \cdot h_l(T) \tag{3}$$

Heat capacity is found by differentiation of enthalpy with respect to temperature. For sufficiently small ΔT of the ice slurry the apparent heat capacity can be estimated with:

$$c_{p\_app} = \left(\frac{\Delta w_i}{\Delta T} \right) \cdot [h_i - \Delta H_f - h_l] + w_i \cdot c_{p\_i} + [1 - w_i] \cdot c_{p\_l} \tag{4}$$

This apparent heat capacity is only valid in situations where ice crystals actually grow or melt. Otherwise the heat capacity is determined using the sensible heat capacities of ice and liquid solution, disregarding the latent heat term of Eq. (4). The apparent heat capacity

undergoes a step change up as the temperature drops below the initial freezing point and ice is formed. At lower temperatures and higher ice fractions the apparent heat capacity of ice slurries decreases gradually.

An empirical model predicting ice slurry *dynamic viscosity* is the model of Thomas [14], which is used by various researchers [2,11]. The dynamic viscosity of a slurry at zero ice fraction of this model is not equal to that of the liquid solution, therefore a factor −1 is included here in the exponential factor of Eq. (5). This causes a minor difference with the model of Thomas at low ice fractions, which however gets smaller at higher ice fractions.

$$\mu_{is} = \mu_l \cdot (1 + 2.5 \cdot \phi_i + 10.05 \cdot \phi_i^2 + 0.00273 \cdot (e^{16.6 \cdot \phi_i} - 1)) \quad (5)$$

Experimental validation by Kauffeld et al. [15] of Eq. (5) for the case of ethanol based ice slurries showed that this model induces considerable errors at ice fractions above 0.20. They assumed that at higher ice fractions ice slurries no longer behave as Newtonian fluids. Property data of solutions used in Eqs. (1)–(5) were obtained from Melinder [16]. In Fig. 7 the relative change of ice slurry properties at increasing ice fraction is given.

2.3. Correlations for prediction of heat transfer in liquid/solid fluidized beds

Many researchers have reported empirical correlations to predict heat transfer in liquid/solid fluidized beds as given in Eq. (6):

$$Nu_p = c_1 Re_p^{c_2} Pr^{c_3} (1-\varepsilon)^{c_4} \varepsilon^{c_5} \left(\frac{d_p}{D}\right)^{c_6} \left(\frac{\rho_s - \rho_l}{\rho_l}\right)^{c_7} \quad (6)$$

A collection of 36 models and 2665 experimental data points was compiled by Jamialahmadi et al. [10]. Based on this collection a generalized model of the form of Eq. (6) was developed by Haid et al. [7]. The following parameters predicted the experimental data of this database with 32.4% average error: $c_1 = 0.1493$, $c_2 = 0.72$, $c_3 = 0.52$, $c_4 = 0.19$, $c_5 = -1.41$, $c_6 = 0.17$, $c_7 = 0.03$.

The model of Eq. (6) was simplified to a model with three constants [9], with an increase of the relative error to 34.4%:

$$Nu_h = c_1 \cdot Re_h^{c_2} Pr^{c_3} \quad (7)$$

with parameters $c_1 = 0.0734$, $c_2 = 0.75$ and $c_3 = 0.63$. The simplified model includes hydraulic Nusselt and Reynolds numbers, which are calculated using Eqs. (8) and (9):

$$Nu_h = \frac{\alpha d_p}{\lambda} \frac{\varepsilon}{1-\varepsilon} \quad (8)$$

$$Re_h = \frac{\rho u_s d_p}{\mu} \frac{1}{1-\varepsilon} \quad (9)$$

A large range of errors was found between different researches: The average error of the model predicting the experimental data was 34.4%, but errors of over a 100% were reported.

Most models in the database of Jamialahmadi et al. [10] were obtained using an electrical heating device to heat the fluidized bed, with the objective of heating the fluid. Coefficients for the case of cooling of a fluid can differ significantly, for example the exponent of the Prandtl number in the Dittus–Boelter model [18], which is 0.3 for heating and 0.4 for cooling applications in tubes.

Some data sets have been reported where the fluids were of relatively high viscosity, as is also the case for ice slurries. For example Kraft black liquor in the research of Bremford et al. [19]. In this paper considerable errors were found if experimental data were compared to the generalized models of Eq. (6). Other models predicted the experimental data more accurately, for example the model of Kim et al. [20]. This model is of the form of Eq. (6) but also includes the *Ar*-number:

$$Nu_p = c_1 Re_p^{c_2} Pr^{c_3} Ar^{c_4} \left(\frac{1-\varepsilon}{\varepsilon}\right)^{c_5} \quad (10)$$

with $c_1 = 0.0722$, $c_2 = 0.25$, $c_3 = 0.5$, $c_4 = 0.25$ and $c_5 = 0.25$.

Models that were fit to experimental data for heat transfer to black liquor gave different results at different black liquor solids concentrations. This indicates that the presence of solids influencing fluid viscosity has considerable impact on heat transfer coefficients.

3. Experimental method

A single tube fluidized bed heat exchanger was used to determine heat transfer coefficients during ice crystallization. Cooling capacity was provided by a secondary fluid which was cooled in a water cooled commercial chiller. Solid particles were separated from the ice slurry on top of the fluidized bed. The ice slurry was collected in a stirred storage tank equipped with a heater to melt the ice. A schematic layout of the fluidized bed test set-up is given in Fig. 2.

Fluidized beds of internal diameters of 43 and 56 mm were tested. The tubes were made of stainless steel with 2 mm wall thickness and a height of 4.6 m. Cylindrical stainless steel particles of 3 and 4 mm, with equal height and diameter, were used. A rotary positive displacement pump was used to pump the slurry through the ice slurry generator and to fluidize the steel particles. All experiments were carried out with the fluidized bed in stationary operation without circulation of solid particles.

In the 43 mm bed a transparent section was installed halfway to observe the fluidization regime. On top of

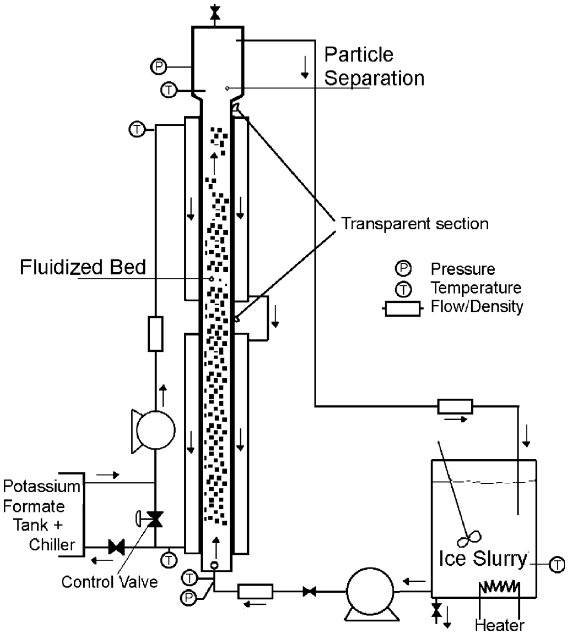

Fig. 2. Experimental set-up for determination of heat transfer coefficients, single tube counter-current fluidized bed.

both fluidized beds transparent sections were used to control the height of the fluidized beds during stationary operation. By weighing of the solid particles present in the fluidized beds before or after experiments, the bed voidage could be accurately determined. A pressure difference transmitter with accuracy of ±1 mbar was installed to measure pressure difference between top and bottom of the fluidized bed. This indicated possible blockages by freezing. The pressure difference is also a measure of the bed voidage, however in the experiments weighing of the particles was used to determine bed voidage.

In the ice slurry storage tank a propeller type stirrer was installed that could keep ice slurries homogeneous up to ice mass fractions of approximately 0.15. At the given chiller capacity, a maximum increase of the ice mass fraction of 0.04 could be obtained for one pass through the fluidized bed. As the ice slurry feed to the fluidized bed is taken from the bottom of the storage tank, the maximum ice mass fraction expected in the fluidized bed is around 0.19. Higher ice mass fractions can be formed in the ice slurry storage tank, where ice crystals then form a floating layer rich of ice. As in the fluidized bed ice slurry generator no ice mass fractions higher than 0.19 are expected, Eq. (5) is considered suitable for viscosity calculations inside the fluidized bed systems.

In the annular space around the fluidized bed a secondary refrigerant without phase change was used. In- and outlet temperatures of this secondary refrigerant, a 34% potassium formate solution with initial freezing point −25 °C, were measured with PT-100 sensors. The sensors were calibrated with an accuracy of ±0.02 K. In and outlet temperatures of the fluidized bed were also measured using PT-100 sensors with ±0.02 K accuracy. Other temperatures were measured with thermocouples type T with accuracy of ±0.05 K. The annular tube was well insulated. Flow rates of ice slurry and secondary refrigerant were measured using Coriolis-type mass flow meters, with accuracy of ±0.1% of the measured value. Also the density of the ice slurry could be determined using the Coriolis-type flow meters, also with accuracy of ±0.1% of the measured value. The enthalpy difference of the secondary refrigerant at the in- and outlet was predicted from the temperature data. Using Eq. (11) the overall heat transfer coefficient, U, was determined.

$$Q = U \cdot A \cdot \Delta T_{\ln} \tag{11}$$

with A the outside surface area of the tube. The wall-to-bed heat transfer coefficient (α_{in}) was then determined with Eq. (12):

$$\frac{1}{U} = \frac{1}{\alpha_{out}} + \frac{d_{out}}{2\lambda_w} \ln\left(\frac{d_{out}}{d_{in}}\right) + \frac{d_{out}}{d_{in}} \cdot \frac{1}{\alpha_{in}} \tag{12}$$

The overall heat transfer resistance ($1/U$) consists of three parts: The annular side heat transfer resistance, the heat transfer resistance of the stainless steel walls and the wall-to-bed heat transfer resistance on the fluidized bed side. The heat transfer coefficient on the annular side was estimated with the model of Gnielinski [21]. For the 56 mm fluidized bed the annular heat transfer coefficient was approximately 2 kW/m^2 K, for the 43 mm fluidized bed this was 4 kW/m^2 K. A reference experiment with pure water and no fluidized bed present indicated that this model determined annular heat transfer coefficients with a maximum error of 12% (6% average error). The temperature measurement error on the ice slurry side needs to be added to this error. The maximum measurement error was up to 20% at low temperature differences. Measurements became more accurate at higher temperature differences between primary cooling fluid and ice slurry.

The freezing point of a liquid solution is determined by the concentration of freezing point depressant. If ice is formed, the concentration of freezing point depressant in the remaining liquid phase increases and the freezing point of this liquid phase decreases, assuming the ice formed consists of pure water. If the ice slurry is in equilibrium, the temperature of the ice slurry then equals the freezing temperature of the liquid phase. The ice fraction can thus be calculated from the initial freezing point depressant mass concentration, $m_{fpd,0}$, and temperature measurements, using the relation between freezing temperature, T_f, and mass concentration freezing point depressant, m_{fpd}:

$$w_i = 1 - \frac{m_{fpd,0}}{m_{fpd}(T_f)} \quad (13)$$

Freezing point data, $m_{fpd}(T_f)$, were obtained from Melinder [16]. Accuracy of this method was confirmed with the Coriolis mass flow and density meters.

In the experiments, two types of freezing point depressing additive were used: Sodium chloride and ethylene glycol. Microscopic pictures used to evaluate size and shape of ice crystals, indicated that ice crystals generated in the fluidized bed system were similar for both additives. Ice crystals were rounded, without sharp edges and shaped like disks. Diameters of ice crystals produced in the fluidized bed were in the range of 0.1–0.3 mm. Possible effects of different size or shape of ice crystals on heat transfer coefficients were assumed to be less relevant in these experiments.

The capacity of the chiller was approximately 5 kW at −10 °C. This formed a limit on the amount of heat that could be transferred, imposing a limit on the temperature difference that could be attained in the set-up. In the ice slurry storage tank a heater of 3.4 kW maximum capacity was installed to melt ice and maintain a constant ice fraction. Initial freezing points of solutions of both freezing point depressants were in the range of −1 to −7 °C.

An ice slurry production run was considered stable if a constant heat transfer coefficient was maintained up to an ice fraction in the tank of at least 0.19. Stable operation also required the fluidized bed to remain fluidized without being blocked by ice or showing an outflow of solid particles. Using the heater, steady-state conditions were assumed after 20 min of ice slurry production without change in heat transfer coefficient or fluidization conditions.

Initial ice nucleation was started in experiments by seeding with small ice crystals after the liquid in the storage tank just became supercooled. In the experimental set-up initial nucleation could also occur without seeding at 0.5–1.5 K of supercooling. To prevent the sudden formation of large ice fractions which might cause instability, seeding was however used in most experiments. Approximately 100 ice slurry production tests were conducted at various operating conditions, 75 of these resulted in stable ice slurry production conditions, suitable for heat transfer calculations.

4. Results and discussion

4.1. Operating range of fluidized bed ice crystal generator

Ice slurry generation in a fluidized bed heat exchanger can only be stable within a certain range of operating conditions. The solid particles need to impact on the heat exchanging surfaces frequent enough to keep them free of ice. Several factors may prevent this:

1. If the temperature driving force is too high, ice crystal growth will be too fast and a solid ice layer will build-up regardless of the impact of solid particles.
2. A too low liquid phase velocity, encountered at low bed voidage, will not give the solid particles enough momentum. The particles can then not impact hard enough on walls to keep ice from sticking to the walls. Ice will also stick to walls if particles are too light or too small.
3. An aggregate fluidization regime or a too high bed voidage might cause parts of the heat exchanging walls to be without particle impacts for too long, allowing for build-up of an ice layer.

Heat transfer rates decrease if there is a solid (growing) layer of ice sticking to the heat exchanging surface. Also the fluidized bed will expand and flow out of the tube, because there is less volume available for the fluidized bed. The fluidized bed operation becomes unstable and it will eventually be completely blocked by ice.

The factors mentioned above are not independent: For each set of operating conditions there appears to be a maximum temperature difference above which ice will stick to walls.

A few parameters are essential to control the generation of ice slurry: The temperature driving force for crystallization, the bed voidage and superficial velocity. Also fluid properties, bed and particle dimensions impose limits on the operating range of the fluidized bed ice generator, as these determine the fluidization regime. In experiments it was found that at a bed voidage of 0.75 or lower there was no stable ice slurry generation possible. Also at a bed voidage of 0.88 ice slurry could only be produced at very low temperature differences. Higher bed voidages may be possible at small temperature differences but were not tested. Optimum heat transfer coefficients have been predicted around a bed voidage of 0.73 by Jamialahmadi et al. [10]. This optimum bed voidage is probably hard to obtain during ice slurry generation. The limits on the operating range complicate determination of an accurate heat transfer model, as some parameters cannot be altered over a wide range.

The maximum allowable wall-to-bed temperature difference strongly depends on the mass concentration of freezing point depressant. At low freezing point depressant mass concentrations ice crystals are more likely to attach to walls and the allowable temperature difference is low. In Fig. 3 wall-to-bed temperature differences are given versus the freezing point depressant concen-

tration for all experiments with sodium chloride at 0.80 bed voidage. The line between stable and unstable ice slurry generation conditions gives the maximum allowable wall-to-bed temperature difference. The limit depends almost linearly on the sodium chloride concentration. It was found that at a higher bed voidage the maximum allowable wall-to-bed temperature difference was smaller than in the experiments of Fig. 3. If ethylene glycol was used as freezing point depressant instead of sodium chloride, the stable operating range was larger. At equal freezing points, approximately 33% larger temperature differences could be applied with ethylene glycol. The limit again depended linearly on the concentration.

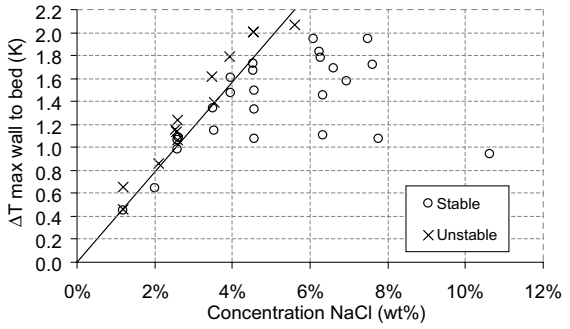

Fig. 3. Maximum wall-to-bed temperature difference for NaCl based ice slurry. Bed voidage of 0.80, 4 mm cylindrical steel particles in 56 mm diameter fluidized bed set-up.

4.2. Thermophysical properties

The thermophysical property models for ice slurries of Section 2.2 combine properties of liquid solution, ice, and their interactions. It is, however, not known if there are interaction effects during ice formation in the fluidized beds. If heat is transferred primarily from walls to the liquid phase of the slurry and ice crystallization occurs in the bulk of the bed, only properties of the liquid phase are required for heat transfer calculations. Otherwise, if the ice slurry behaves as a single fluid, property models of the ice slurry including the solid ice phase need to be used.

In Fig. 4 heat transfer results of a typical production run are displayed for an ice slurry based on sodium chloride. Also the ice fraction at the outlet of the fluidized bed heat exchanger is displayed in Fig. 4. In this experiment the inlet temperature of the secondary refrigerant was kept constant. At higher ice fractions the temperature of the ice slurry decreases as the freezing point is further depressed, therefore the overall temperature difference slightly decreases. In other experiments the primary cooling fluid temperature was adjusted to obtain a constant overall temperature difference. The experiment was stopped at an ice mass fraction of approximately 0.17. The heat transfer coefficient is practically constant. The average heat transfer coefficient is calculated for comparison with other experiments.

In Fig. 5 the range of the average heat transfer coefficient is given for the experiments with NaCl in the 56 mm diameter tube and for the experiments with ethylene glycol in both the 43 mm and the 56 mm tube. Heat

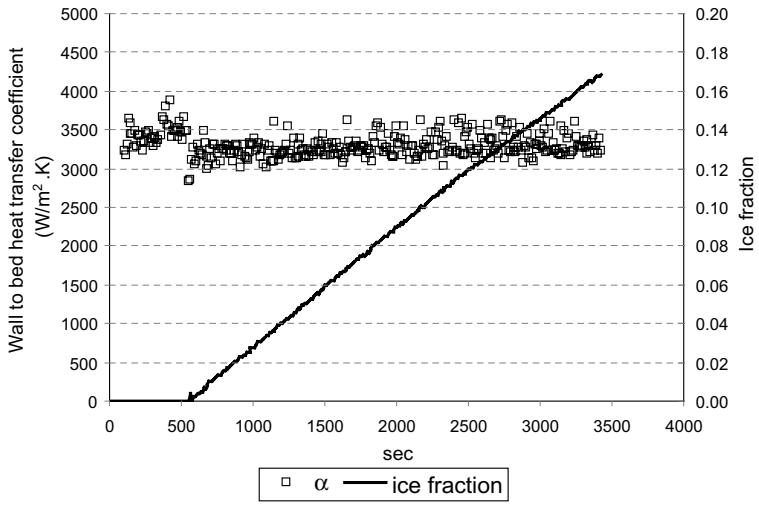

Fig. 4. Wall-to-bed heat transfer and ice fraction for NaCl ice slurry production run in 56 mm diameter fluidized bed with 4 mm particles and 0.80 bed voidage. NaCl concentration: 6.6 wt%, −4.1 °C initial freezing point. Ice crystallization starts at $t = 500$ s.

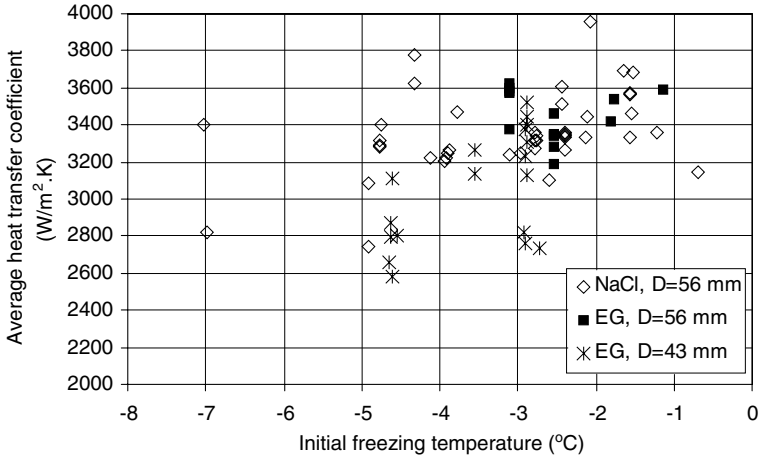

Fig. 5. Overview of the average heat transfer coefficients versus the initial ice slurry freezing temperature. Experiments with ice slurries based on NaCl and on ethylene glycol in the 56 mm diameter fluidized bed with 4 mm particles and with ice slurries based on ethylene glycol in the 43 mm diameter fluidized bed with 3 mm particles.

transfer coefficients appear higher at higher freezing temperatures, but effects of other significant parameters, such as bed voidage and superficial velocity, are not shown in Fig. 5. The heat transfer coefficients are plotted versus the superficial velocity in Fig. 6 for the same experiments as in Fig. 5. The heat transfer coefficients predicted with the Dittus–Boelter model [18] for fluids with similar thermophysical properties but in single phase flow without fluidized bed, are also shown in Fig. 6. The heat transfer coefficients are significantly higher with the fluidized bed present, which is consistent with earlier work on fluidized bed heat transfer [7]. It should be noted that it is not possible to produce ice slurry without the fluidized bed.

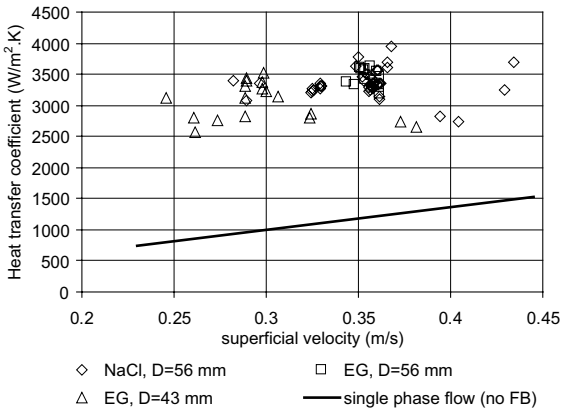

Fig. 6. Overview of the average heat transfer coefficients versus the superficial velocity in the fluidized bed. Results of the same experiments as displayed in Fig. 5, with heat transfer coefficients under equal conditions without fluidized bed.

In the experiment of Fig. 4 the heater in the ice storage tank was not used, so effects of an increasing ice fraction could be observed. The heat transfer coefficient remained at a practically constant level at increasing ice fraction. As temperature differences and ice fractions only change very gradually, the system was assumed near steady state for heat transfer calculations. To obtain a true steady state however, the heater is required to melt the ice crystals produced. A number of experiments have been performed under constant ice fraction conditions.

The general model of Eq. (7) was used to initially examine heat transfer trends at increasing ice fractions. This generalized model was considered suitable as an initial model to test effects of different thermophysical properties, as it was obtained from researches under a wide range of conditions. If the apparent heat capacity including the latent heat effect is used in this model to calculate the Prandtl number, a step change up to more than double the heat transfer coefficient would be seen after the start of ice formation. In the experimental data however no such step could be identified, as can be seen in Fig. 4. Instead a small step down is observed, which is caused by the different temperature of the ice slurry as the supercooling substantially decreases after the start of ice formation. The Prandtl number at the start of ice formation calculated with apparent heat capacity in this experiment is 309, which predicts a heat transfer coefficient of 4.0×10^4 W/m^2 K, using Eq. (7). Such a large heat transfer coefficient was not observed in the experiments. The Prandtl number calculated with the sensible heat capacity only is 14.5, which predicts a heat transfer coefficient of 6.05×10^3 W/m^2 K, which is more consistent with the heat transfer coefficient measured of 3.09×10^3 W/m^2 K. The latent heat effect of the phase

change was therefore disregarded and only sensible heat of the liquid phase and the sensible heat of the ice are relevant for heat transfer calculations. Eq. (7) then still overpredicts heat transfer coefficients during ice formation, but is within the error range of the models that were used to obtain the generalized equation, where the models of individual researches could differ up to 100% higher or lower [7].

Viscosity of ice slurries is higher when ice fractions increase, according to Eq. (5). If the model of Eq. (7) is used, this would imply a decreasing heat transfer coefficient at higher ice fractions, as viscosity has a sum of exponents of −0.12. Thermal conductivity increases at higher ice fractions according to Eq. (2), which would give higher heat transfer coefficients because of a total exponent of 0.37. These two effects cancel each other at low ice fractions. At higher ice fractions the viscosity effect is dominant and heat transfer coefficients are predicted to decrease. The density and the sensible heat capacity only slightly change at higher ice fractions and are less influential in heat transfer models. In Fig. 7 the relative change of properties at increasing ice fraction is given for ice slurry with NaCl as the freezing point depressant, with initial concentration of 10 wt%, and an initial freezing point of −6.6 °C.

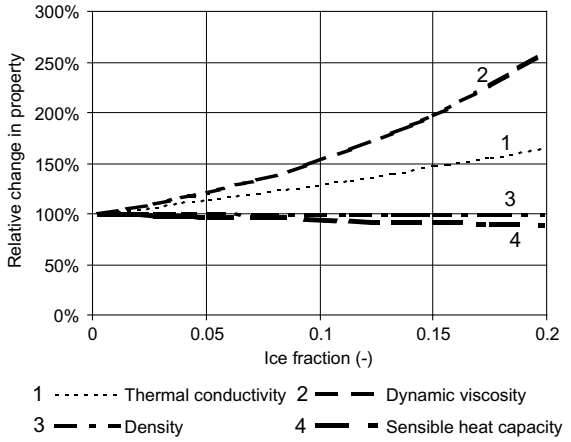

Fig. 7. Relative change of ice slurry properties at increasing ice fraction. For ice slurries based on 10 wt%. NaCl, initial freezing temperature −6.6 °C.

In Fig. 8 heat transfer coefficients calculated with Eq. (7) for the experimental conditions of Fig. 4 are displayed. Also heat transfer coefficients calculated with thermophysical properties of only the liquid phase of the ice slurries are displayed, which would be valid if ice crystals would not affect heat transfer. Both curves are very similar; relative difference between the curves is smaller than 2%. The curves do not provide enough detail to be certain about the type of thermophysical property models that need to be used. At low ice fractions, the influence of ice crystals appears to be relatively unimportant for the heat transfer coefficients in the fluidized bed ice slurry generator. Thermophysical property models of the ice slurry as a single fluid, including the solid ice properties, are used in the next section to obtain an accurate heat transfer model. These predict a more constant heat transfer coefficient than if only the properties of the liquid phase were used. This is more consistent with the experimental results.

At higher ice mass fractions both curves predict a slightly decreasing heat transfer coefficient. In the experiments however this was not observed. Instead, heat transfer coefficients increased slightly at higher ice fractions, as can be seen in Fig. 4. The ice particles

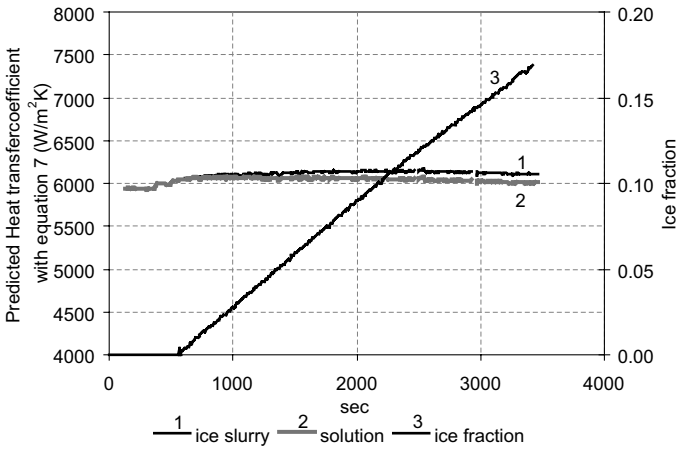

Fig. 8. Estimated heat transfer coefficients with Eq. (7) using thermophysical properties of ice slurry and of liquid solution at increasing ice fraction. Conditions as in Fig. 4.

themselves might have a positive effect on heat transfer, similar to those of the inert steel particles. The effect is small and could also be caused by the slightly different temperature levels at higher ice fractions. Furthermore, this slightly increasing trend was not obvious in all experiments.

4.3. Heat transfer model

Because of the practical limits of ice slurry generation in the fluidized beds, discussed in Section 4.1, the bed voidage and the ice slurry temperatures were altered over a relatively small range. Some parameters concerning system dimensions were not varied. If not enough experimental data were obtained to get a meaningful fit value for exponents of these parameters, literature values were used. For example the ratio between the particle diameter and the column diameter was hardly varied in experiments, as in the smaller diameter fluidized bed also smaller steel particles were used. In Table 1 an overview of the range of operating parameters is given.

The heat transfer data obtained were compared with predictions of literature models of Eqs. (6), (7) and (10) and with some literature models that were used to obtain the generalized correlations [17,22–24]. Results are given in Table 2. The literature models overpredict the experimental results with 21–90%. These differences are large, but are within the range of errors of the individual researches that were used to obtain the generalized models of Eqs. (6) and (7) [7].

If the proportional factor, c_1, in the models is adjusted, accuracy of models is improved and more acceptable error levels are obtained. If all exponents of Eqs. (6) and (7) are used as parameters for fitting with a least sum of squares method, accuracy is further improved, as is displayed in Table 2. The resulting coefficients for the Reynolds and Prandtl numbers are close to those of the literature models. Trends in heat transfer during ice slurry production are therefore similar to heat transfer without ice, only the proportional coefficient is different.

Table 1
Range of operating parameters

Parameter	Min.	Max.
Re_p (–)	205	1060
Pr (–)	13	29
ε (–)	0.77	0.88
d_p (m)	0.003	0.004
D_h (m)	0.043	0.056
u_s (m/s)	0.25	0.44
T (K)	266	272
m_{fpd} (wt%)	1.2	13.2
w_i (–)	0	0.19
μ_{is} (Pa s)	0.0017	0.0045
λ_{is} (W/m K)	0.53	0.69
ρ_{is} (kg/m^3)	995	1080
c_{p_is} (kJ/kg K)	3.63	4.16
Nu_p (–)	16	30
α (W/m^2 K)	2580	3950

The model similar to Eq. (7), with fit parameters, $c_1 = 0.0587$, $c_2 = 0.709$ and $c_3 = 0.622$ gave the most accurate predictions. Nusselt numbers predicted for all the experiments with stable ice slurry production are displayed in Fig. 9, corresponding heat transfer coefficients in Fig. 10.

Typically literature models overpredict heat transfer coefficients during ice generation with a proportional factor. A likely cause might be interference of ice crystals or interference of the ice crystallization process. However, heat transfer coefficients just before start of ice formation are similar or almost equal to heat transfer coefficients just after start of ice formation, which can be seen in Fig. 4. Heat transfer coefficients appear slightly lower after start of ice crystallization at $t = 500$ s, but the difference is 10% at most. Formation of ice crystals is therefore not causing the lower heat transfer coefficients and there is no semi-permanent ice layer present on the walls of the fluidized beds. There could however still be small ice nuclei at the walls that have only a minor impact on heat transfer coefficients.

Another reason for the difference with the literature models might be the temperature levels close to the freezing point of the solutions. Viscosity of solutions is relatively high close to the freezing point and a high viscosity is a likely cause for modified behavior, as was reported by Bremford et al. [19]. Temperature levels of the various researches were typically above 300, 28–34 K higher than in the current research. An experiment measuring heat transfer coefficients at higher temperatures was conducted to compare heat transfer coefficients at conditions more similar to the various literature researches. The difference in the proportional factor was reduced considerably at higher temperatures, as can be seen in Table 3. In this table experimental heat transfer coefficients at temperatures between 0 and 22 °C are compared with the model of Haid of Eq. (7). This generalized model already slightly overpredicted the experimental data discussed in Haid et al. [7], which also explains the differences partially. In the current ice slurry experiments the generalized model of Eq. (7) also predicted relatively high heat transfer coefficients compared to some other models [22–24].

Another possible cause for differences is the heat transfer determination method. Most literature models use an electrical heater for heating of a fluidized bed to determine heat transfer coefficients, while in current experiments cooling with a fluid is used.

In the models of Eqs. (6) and (7), both column diameter and particle diameter influence the heat transfer

Table 2
Comparison of literature heat transfer models and least square fits of Eqs. (6), (7) and (10) applied to all experimental data for ice slurry generation

Model	Parameters							Rel. avg. error	R^2
	c_1	c_2	c_3	c_4	c_5	c_6	c_7		
Haid [9] (Eq. (7))	0.0734	0.75	0.63	–	–	–	–	78%	–
Adjusted c_1	0.0412	0.75	0.63	–	–	–	–	5.6%	0.912
Lsq fit $c_1, \ldots, c_3$	0.0587	0.709	0.622	–	–	–	–	5.3%	0.917
Haid et al. [7] (Eq. (6))	0.1493	0.72	0.52	0.19	−1.41	0.03	0.17	81%	–
Adjusted c_1	0.0816	0.72	0.52	0.19	−1.41	0.03	0.17	5.8%	0.791
Lsq fit $c_1, \ldots, c_3$	0.085	0.675	0.610	0.19	−1.41	0.03	0.17	5.3%	0.827
Kim et al. [20] (Eq. (10))	0.0722	0.25	0.5	0.25	0.25	–	–	28%	–
Adjusted c_1	0.0557	0.25	0.5	0.25	0.25	–	–	6.0%	0.780
Lsq fit $c_1, \ldots, c_4$	0.0447	0.364	0.659	0.180	0.25	–	–	5.3%	0.836
Rückenstein et al. [17] (Eq. (10))	0.067	−0.237	0.33	0.522	–	–	–	90%	–
Adjusted c_1	0.034	−0.237	0.33	0.522	–	–	–	8.5%	0.561
Lsq fit $c_1, \ldots, c_4$	0.0165	0.0685	0.6955	0.4219	–	–	–	5.9%	0.807
Kang et al. [22] (Eq. (6))	0.191	0.69	0.33	0.31	−1	–	–	21%	–
Adjusted c_1	0.155	0.69	0.33	0.31	−1	–	–	7.0%	0.699
Lsq fit $c_1, \ldots, c_4$	0.0767	0.662	0.594	0.223	−1	–	–	5.3%	0.826
Muroyama et al. [23][a] (Eq. (6))	0.137	0.729	0.33	0.271	−1	–	–	46%	–
Adjusted c_1	0.0926	0.729	0.33	0.271	−1	–	–	7.5%	0.624
Kollbach [24][a] (Eq. (6))	0.118	0.7	0.5	0.2	−1	–	–	56%	–
Adjusted c_1	0.0753	0.7	0.5	0.2	−1	–	–	5.8%	0.794

[a] Least squares fit parameters are the same as for the model of Kang et al. [22].

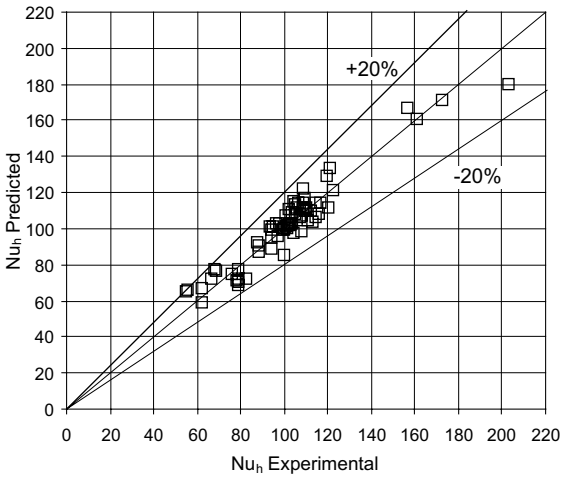

Fig. 9. Comparison of experimental and predicted values of hydraulic Nusselt number with Eq. (7) and lsq-fit model. +20% and −20% margins; $R^2 = 0.917$; avg. error = 5.6%; max. error = 18.4%.

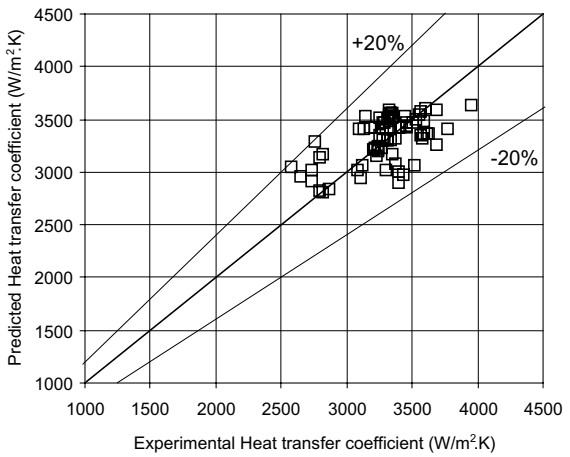

Fig. 10. Comparison of experimental and predicted values of heat transfer coefficient with Eq. (7) and the +20% and −20% margins.

only indirectly, as these parameters codetermine superficial velocity and bed voidage. It is likely that parameters such as column diameter and particle diameter also have a significant impact and can also partially explain differences found in the proportional factor.

Table 3
Comparison of heat transfer coefficients at steady state with Haid model of Eq. (7) in 2–22 °C temperature range

Exp.	Average temp. slurry (no ice), °C	Experimental heat transfer, W/m^2 K	Predicted heat transfer, W/m^2 K	Relative difference
1	22.2	4988	6355	27%
2	15.2	4434	6540	47%
3	12.5	4117	5775	40%
4	8.7	3678	6176	68%
5	7.5	3092	5609	81%
6	2.2	2820	5230	86%

5. Conclusion

The formation of ice crystals did not have a large effect on heat transfer coefficients in the fluidized bed ice slurry generator. If at a given set of operating conditions stable ice slurry production was possible, heat transfer coefficients were similar to those in fluidized beds before start of ice crystal formation. Heat transfer coefficients measured using the fluidized beds were significantly higher than those predicted for single phase flow.

A range of temperature differences was determined in which stable ice slurry generation was possible. The limit of this range depended linearly on the concentration of freezing point depressant.

Thermophysical property models reported for ice slurries in literature could be applied in models to predict wall-to-bed heat transfer coefficients. The heat capacity without the latent heat term should be used for this. An empirical model using hydraulic Nusselt and Reynolds numbers was proposed that predicted heat transfer coefficients in the fluidized bed ice slurry generator accurately. Exponents of this model were similar to those of generalized models found in literature. Significant differences were only found in the proportional factor. Relatively low temperature levels during ice slurry production were the most likely cause for the differences, as no influence of ice crystals was observed.

References

[1] T. Inada, X. Zhang, A. Yabe, Y. Kozawa, Active control of phase change from supercooled water to ice by ultrasonic vibration 1. Control of freezing temperature, Int. J. Heat Mass Transfer 44 (23) (2001) 4523–4531.

[2] O. Bel, A. Lallemand, Study of a two phase secondary refrigerant: intrinsic thermophysical properties of an ice slurry, Int. J. Refriger. 22 (3) (1999) 164–174.

[3] B.D. Knodel, D.M. France, U.S. Choi, M.W. Wambsganss, Heat transfer and pressure drop in ice-water slurries, Appl. Thermal Eng. 20 (2000) 671–685.

[4] J. Bellas, I. Chaer, S.A. Tassou, Heat transfer and pressure drop of ice slurries in plate heat exchangers, Appl. Thermal Eng. 22 (7) (2002) 721–732.

[5] R. Rautenbach, T. Katz, Survey of long time behavior and costs of industrial fluidized bed heat exchangers, Desalination 108 (1996) 335–344.

[6] D.G. Klaren, Self cleaning heat exchangers, in: H. Müller-Steinhagen (Ed.), Handbook Heat Exchanger Fouling: Mitigation and Cleaning Technologies, Rugby Institution of Chemical Engineers, 2000, pp. 186–199.

[7] M. Haid, H. Martin, H. Müller-Steinhagen, Heat transfer to liquid–solid fluidized beds, Chem. Eng. Process. 33 (1994) 211–225.

[8] D.G. Klaren, J.S. van der Meer, A fluidized bed chiller: a new approach in making slush-ice, Industrial Energy Technology Conference Houston Proceedings, Texas A and M University, 1991.

[9] M. Haid, Correlations for the prediction of heat transfer to liquid–solid fluidized beds, Chem. Eng. Process. 36 (1997) 143–147.

[10] M. Jamialahmadi, M.R. Malayeri, H. Müller-Steinhagen, A unified correlation for the prediction of heat transfer coefficients in liquid/solid fluidized bed systems, Trans. ASME, J. Heat Transfer 118 (1996) 952–959.

[11] K.G. Christensen, M. Kauffeld, Heat transfer measurements with ice slurry, in: IIR commission B1 with E1 & E2 conference proceedings, College Park, USA, 1997, pp. 161–175.

[12] M.A. Ben Lakhdar, Comportement thermo-hydraulique d'un fluide frigoporteur diphasique: Le coulis de glace, Ph.D. Thesis, INSA de Lyon, France, 1998.

[13] Tareef, cited in: R.H. Perry, C.H. Chilton, Chemical Engineers Handbook, fifth ed., McGraw-Hill, NY, 1973.

[14] D.G. Thomas, Transport characteristics of suspension: VIII, J. Colloid Sci. 20 (1965) 267–277.

[15] M. Kauffeld, K.G. Christensen, S. Lund, T.M. Hansen, Experience with ice slurry, in: Proceedings of the 1st workshop on Ice Slurries, Yverdon-les-Bains, Switzerland, 1999, IIR, Paris, pp. 42–73.

[16] A. Melinder, Thermophysical properties of liquid secondary refrigerants, Handbook no. 12 of the Swedish Society of Refrigeration, Stockholm, 1997.

[17] E. Rückenstein, V. Shorr, G. Suciu, Despre transferul de caldura dintre un strat fluidizat cu lichid si peretele vasului care-l contine, Studii cercetari fizica, Akad. Rep. Populare Romine 10 (1959) 235.

[18] Dittus/Boelter cited in: J.P. Holman, Heat Transfer, eighth ed., McGraw-Hill, 1997 (Chapter 6).

[19] D.J. Bremford, H. Müller-Steinhagen, G.G. Duffy, Heat transfer to kraft black liquor in a liquid–solid fluidized bed, Heat Transfer Eng. 21 (2000) 57–69.

[20] S.D. Kim, Y. Kang, H.K. Kwon, Heat transfer characteristics in two and three phase slurry fluidized beds, AIChE J. 32 (1986) 1397–1400.

[21] VDI, VDI Wärmeatlas: Berechnungsblatter für den Wärmeübergang, 7e Ed., VDI, Düsseldorf, 1994.

[22] Y. Kang, L.T. Fan, S.D. Kim, Immersed heater to bed heat transfer in liquid–solid fluidized beds, AIChE J. 37 (7) (1991) 1101–1106.

[23] K. Muroyama, M. Fukuma, A. Yasumishi, Wall-to-bed—heat transfer in liquid–solid and gas–liquid–solid fluidized beds part 1, Can. J. Chem. Eng. 64 (3) (1986) 399–418.
[24] J.S. Kollbach, Entwicklung eines Verdampfungsverfahrens mit Wirbelschicht warme austauscher zum eindampfen krustenbildender Abwasser, Ph.D. Thesis, Universität Aachen, 1987.
[25] C. van Heerdan, A.P.P. Nobel, D.W. van Krevelen, Mechanism of heat transfer in fluidized beds, Ind. Eng. Chem. 45 (1953) 1237.